Local structural order in the disordered vanadium tetracyanoethylene room-temperature molecule-based magnet

D. Haskel,[1,*] Z. Islam,[1] J. Lang,[1] C. Kmety,[1] G. Srajer,[1] K. I. Pokhodnya,[2,3] A. J. Epstein,[2] and Joel S. Miller[3]

[1]*Advanced Photon Source, Argonne National Laboratory, Argonne, Illinois 60439, USA*

[2]*Department of Physics and Department of Chemistry, The Ohio State University, Columbus, Ohio, 43210-1106, USA*

[3]*Department of Chemistry, University of Utah, Salt Lake City, Utah 84112-0850, USA*

We determined the vanadium oxidation state and local coordination environment in disordered samples of magnetic $V[TCNE]_x (x \approx 2)$ prepared by chemical vapor deposition (CVD). Systematic studies of the x-ray absorption near-edge structure (XANES) in this material and reference compounds show that V ions have a valence state near 2+. Extended x-ray absorption fine structure (EXAFS) analysis shows that vanadium ions are coordinated by 6.04 ± 0.25 nitrogen atoms at a room-temperature average distance of 2.084(5)Å. The local environment is well defined with a distribution of V-N bond lengths comparable to that commonly found in ordered compounds. This distribution is mostly vibrational in origin, with static contributions being at least four fold smaller. The small disorder in V-N distances is a consequence of strong binding between V and TCNE, with an effective local force constant of $k=87$ N/m. This strong bonding leads to strong nearest neighbor coupling, which for the extended structure of $V[TCNE]_x$ with six N nearest neighbors results in magnetic ordering above room temperature. The strong V-N bonding explains in part the insoluble nature of this compared to other molecule-based magnets. The room-temperature XANES and EXAFS results for the CVD-prepared samples are compared to those for $V[TCNE]_x$ prepared as a powder from CH_2Cl_2 solvent, which has a similar magnetic ordering temperature but a magnetization that is more strongly temperature dependent. This comparison suggests that coordination of 6 nitrogens around each V(II) with little variation in the V-N distances is important for achieving the high magnetic ordering temperature of 400 K associated with samples made by both the CVD and CH_2Cl_2 solution methods.

I. INTRODUCTION

The organic molecule-based magnet vanadium tetracyanoethylene ($V[TCNE]_x, x \approx 2$) is remarkable in that it shows spontaneous ordering of magnetic moments above room temperature ($T_c \sim 400$ K).[1] The magnetic ordering temperature and the temperature dependence of the magnetization $M(T)$ below T_c vary with method of preparation.[1] Vanadium tetracyanoethylene prepared in a CH_2Cl_2 solvent using either $V(C_6H_6)_2$[1] or $V(CO)_6$[2] as a starting material have a T_c of ~ 400 K though samples prepared using $V(C_6H_6)_2$ have a more strongly temperature-dependent $M(T)$ typical of more disordered materials. In contrast, synthesis of $V[TCNE]_x$ prepared in C_4H_8O solvent yields $T_c \sim 240$ K while from CH_3CN solvent yields T_c in the range of 60 to 120 K.[1] Note that, while CH_2Cl_2 does not coordinate with V, C_4H_8O, and CH_3CN do, increasing the disorder and decreasing the number of nearest neighbor spin-carrying TCNE sites. The preparation of $V[TCNE]_x$ using solvent-free chemical vapor deposition (CVD) methodology with $V(CO)_6$ and TCNE as the starting materials yields the same $T_c \sim 400$ K with a $M(T)$ more typical of an ordered magnet[3]. Studies of critical behavior and scaling of $V[TCNE]_x$ prepared in C_4H_8O[4] and CH_3CN[5] solvents and via CVD[6] reveal decreased randomness in the local magnetic anisotropy that correlates with increasing T_c. Note that $Mn[TCNE]_x$ and $Fe[TCNE]_x$ have a T_c of ~ 75 and ~ 100 K, respectively, demonstrating the richness of magnetic behaviors possible in this materials class.[7,8]

Magnetoresistance studies of $V[TCNE]_x$ show an unusual linear behavior on magnetic field below T_c and quadratic magnetoresistance field response for samples above T_c.[9] This has been analyzed in terms of a model of a half-semiconductor with fully spin-polarized valence and conduction bands. Such materials may be suitable for spintronics applications.[9] The incorporation of Co for V in $V_xCo_{1-x}[TCNE]_x$ enables the enhancement of the coercive field.[10] Studies of $Mn[TCNE]_x$ show that exposure to light can increase or decrease the magnetic susceptibility in the magnetic state.[11] It is important to understand the local atomic coordination environment of vanadium, as well as its oxidation state in this compound. This is key for understanding the nature of the chemical bonding, magnetic interactions, and charge transport among vanadium and TCNE ions.

The lack of progress in understanding the structure of $V[TCNE]_x$ is due to its disordered nature and its air sensitivity. Structural characterization requires the ability to probe short-range order in the arrangement of atoms without the requirement of long-range crystalline order. Additionally, theoretical approaches have been limited by the lack of structural information. "Almost nothing is known about the actual structure of the V-TCNE" ferrimagnet, wrote Tchougreeff and Hoffmann in their theoretical analysis,[12] in which a direct interaction between V and eight N atoms from eight surrounding TCNE molecules was assumed. While the medium-range structural ordering remains elusive, herein we report x-ray absorption studies aimed at determining the valence state and local structure of vanadium in $V[TCNE]_x$.

X-ray absorption techniques are well suited for obtaining local electronic and structural information.[13] X-ray absorp-

tion involves the excitation of a tightly bound core electron into available (empty) electronic states. Since the transition probability, given by Fermi's Golden Rule, involves the overlap between the initial core (atomic) and final excited (molecular) electronic states, the x-ray measurements provide information on the local electronic structure at the absorbing atom site (local density of states). The x-ray absorption near edge structure (XANES) is particularly sensitive to changes in the absorbing atom's chemical valence state. Such changes cause chemical shifts in the absorption threshold which can be used to determine valence state by comparing to standards. The XANES also contains structural information, but a quantitative analysis requires accounting for a large number of single and multiple scattering events. This is due to the strong scattering amplitudes and long photoelectron mean free path that occur at low energies.

The extended x-ray absorption fine structure (EXAFS), i.e., the fine structure on the x-ray absorption coefficient at higher excitation energies relative to the absorption edge, is easier to interpret as the limited photoelectron mean free path (≈ 10 Å) and weaker scattering amplitudes result in contributions from a smaller number of scattering events. This fine structure, which is due to the modification of the photoelectron wave by scattering from the potential of neighboring atoms, originates in a small cluster of atoms surrounding the absorbing atom. As such, it does not require long-range crystalline order and is therefore ideal for studies of amorphous materials. In the case of $V[TCNE]_x$, the element specificity intrinsic to this technique allows us to determine the local atomic environment about the vanadium atoms.

The paper is organized as follows: in Sec. II we describe the experimental details. In Sec. III we show XANES measurements for structurally related V-containing model compounds with known valence states and compare them to $V[TCNE]_x$. This enables the determination of the oxidation state of V. In addition, we illustrate the importance of using appropriate standards by showing that comparison with highly ionic vanadium oxides results in an unphysical vanadium oxidation state. In Sec. IV we present EXAFS measurements on $V[TCNE]_x$ samples together with those of model compounds with known coordination environments. The implications of our results are discussed in Sec. V, and are summarized in Sec. VI.

II. EXPERIMENTAL

The $V[TCNE]_x$ used in this study was grown by the CVD technique as thin films, a few microns thick, on glass substrates.[3] Due to the relatively low rate of deposition ($\approx 1-5 \mu m$ in 12 h) repeated depositions were required to obtain enough material for the x-ray absorption measurements. These are optimized for a sample thickness of $\approx 80 \mu m$, giving an absorption edge jump $\Delta \mu x \approx 1$ at the V K-edge. Here μ is the absorption coefficient and x the sample thickness. The deposited films were used to make powder samples, which were mixed with Apiezon N grease and cast into disk shapes by embedding in 1-mm-thick aluminum washers. The effective thickness of the sample was nearly ideal, as determined from the measured absorption

edge jump. Since $V[TCNE]_x$ is very air sensitive, sample preparation was done in Vacuum Atmospheres Drilab ($\lesssim 0.5$ ppm O_2; $\lesssim 0.5$ ppm H_2O) under nitrogen. Samples used as XANES standards were also in powder form, uniformly dispersed in Apiezon N grease. These include $[N(C_2H_5)_4][V^{-I}(CO)_6]$, $V^0(CO)_6$,[14] six coordinated $[V^{II}(NCCH_3)_6][B(C_6H_5)_4]_2$,[15] $V^{II}(OH_2)_6(SO_4)$,[16] $V^{III}_2 \times (SO_4)_3$,[17] and $V^{IV}O(Pc)(Pc=C_{32}H_{16}N_8)$ (Aldrich). The VOPc sample was also used as an EXAFS standard for five coordination, as well as $V^{III}Cl_3(THF)_3$ (THF$=OC_4H_8$) for six coordination,[18] and $(NH_4)_3[V^VS_4]$ for four coordination[19] about the central V ion. The XANES data were also measured on $V^{II}O$, $V^{III}_2O_3$, $V^{IV}O_2$, and $V^V_2O_5$ oxide powders (Alfa Aesar).

X-ray absorption measurements at the V K-edge ($1s$ electron excitation) were done at beamline 4-ID-D of the Advanced Photon Source at the Argonne National Laboratory. Undulator radiation was monochromatized with Si(111) double-crystal monochromators. Harmonic rejection was achieved by double reflections from Pd-coated mirrors at an 8 mrad incidence angle. Measurements on all samples were done in transmission geometry by monitoring the incident and transmitted intensity before and after the sample with highly linear x-ray ionization chambers. For the low-temperature measurements, the "washer" samples were in thermal contact with the cold finger of a closed cycle displex refrigerator. Samples were enclosed in a Be can filled with He exchange gas to prevent air exposure and provide better thermal contact. The stability of $V[TCNE]_x$ was verified through the reproducibility of XANES measurements as well as from magnetization measurements before and after the x-ray experiments. The x-ray energy was calibrated with a vanadium metal foil whose maximum derivative in the absorption spectrum was set to 5.464 keV. The energy resolution in our measurement is estimated at 0.5 eV.

III. VALENCE STATE OF VANADIUM: XANES MEASUREMENTS AND RESULTS

Figure 1 shows room-temperature, normalized $V[TCNE]_x$ XANES data at the V K-edge (top) together with its derivative (bottom). Features A and B in the spectrum are assigned following Wong *et al.*[20] and references therein. Feature A at the threshold (the first peak in the derivative spectrum) corresponds to a $1s \rightarrow 3d$ transition. Generally, if a center of inversion (*i*) exists at the absorbing site, this transition is strictly dipole forbidden since electric dipole transitions require $\Delta l = \pm 1$, where l is angular momentum. Although allowed as an electric-quadrupole transition, the much weaker oscillator strength of quadrupole transitions cannot explain the observed pre-edge peak intensity in this and other vanadium compounds.[20]

In the case of vanadium oxide ($V^{II}O$), where V is at the center of a regular octahedron having rigorous inversion symmetry[20] (Fig. 2, top left), feature A is absent. However, when the site symmetry is lowered and the inversion center is broken, such as in the distorted octahedral environment of $V^{III}_2O_3$ and $V^{IV}O_2$, and the distorted square pyramidal of
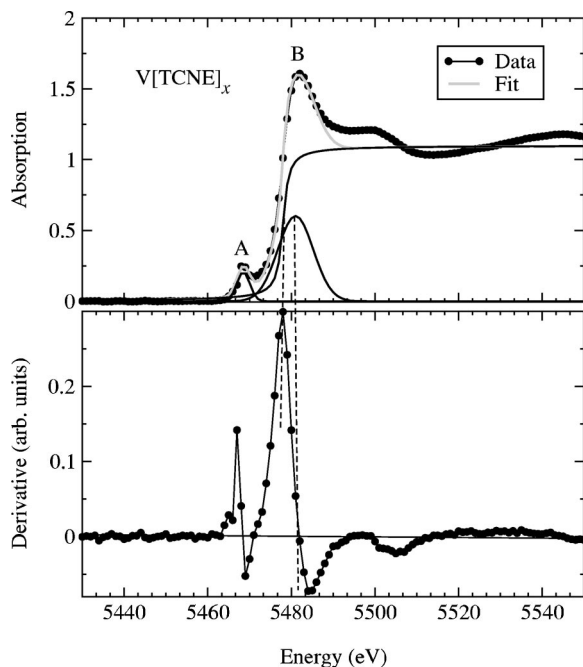
FIG. 1. XANES data (top) and its derivative (bottom) for the V K-edge of V[TCNE]$_x$. Features A and B correspond to transitions into electronic states with a $3d$, $4p$ orbital character, respectively(Ref. 20). Chemical shifts in the absorption edge (maximum derivative) and feature B (Gaussian centroid) for several compounds with known oxidation states were used to infer the oxidation state of V in V[TCNE]$_x$ (see the text).

V$^V_2$O$_5$,[20] this transition becomes dipole allowed due to $3d$-$4p$ mixing. An increased overlap between metal $3d$ orbitals and oxygen $2p$ orbitals due to shorter V-O distances in the noncentrosymmetric structures also contributes to enhancements in this peak. The presence of a sizable pre-edge feature (A) in V[TCNE]$_x$ indicates the absence of inversion symmetry at the V site. We note that the size of this feature in V[TCNE]$_x$ is comparable to that measured in a V^0(CO)$_6$ standard (shown later in Fig. 7). There the octahedral symmetry is weakly broken with a spread in neighboring distances of less than 0.01 Å about a 2.0 Å average distance.[21] Since such small distortions cannot be resolved in the refinements of EXAFS data due to the inherent small spatial resolution of EXAFS in amorphous samples, the extreme sensitivity of XANES to this broken symmetry provides a unique structural (albeit qualitative) characterization tool.

Feature B is assigned to dipole-allowed $1s \rightarrow 4p$ transitions. The XANES data near the threshold are well reproduced by fitting the data with two Gaussians for features A and B superimposed on an arctangent function used to simulate the absorption edge jump. The energy positions of these features depend on the oxidation state. For example, the position of the absorption edge, given by the centroid of the arctangent (or the maximum in the derivative spectrum), will shift to higher energies with an increasing valence state due to the increased attraction of the $1s$ electron to the nucleus and reduced repulsive interactions with the other electrons. Since the outermost $4p$ levels are less tightly bound and hence more affected by changes in the valence state, feature

B is most sensitive to changes in the oxidation state.

Figure 2, lower panel, shows the energy of the absorption edge, determined from the centroid of the arctangent function and the energy of feature B, determined from its Gaussian centroid (squares) or the related zero crossing of the derivative spectrum (points) for a series of vanadium oxides standards (left) and molecular standards (right) with known V oxidation states. The equivalent information for V[TCNE]$_x$ is shown with circles on the right panel. The energy shift per unit of valence increase is obtained from the slope of the fitted lines through the data points and shows a larger sensitivity for the transition into $4p$ final states (3.1 and 4.8 eV/valence for the oxides and molecular standards, respectively) compared to shifts in the absorption edge (2.0, 1.8 eV/valence for the oxides and molecular standards, respectively). The oxides values are in excellent agreement with previously reported data.[20] An interpolation of the V[TCNE]$_x$ results (circles) into those of the molecular standards yields a valence state for V of 2.25±0.25. The major source of error is attributed to the variations in the type of coordinating atom. Nevertheless, the molecular standards provide a greater degree of self consistency in the result obtained from different absorption features, in contrast to the oxide standards. Interpolation into the results from the latter gives inconsistent oxidation states of 0.8 or 3.0, based on chemical shifts of feature B or the absorption edge, respectively. This discrepancy is not surprising as the nature of bonding in the molecular compounds (greater covalency and bonding to similar atoms with similar hybridization) is a better model for the bonding that occurs in V[TCNE]$_x$.

IV. LOCAL ENVIRONMENT OF VANADIUM: EXAFS MEASUREMENTS AND RESULTS

The cross section for photoelectric x-ray absorption past an absorption edge exhibits an energy-dependent fine structure due to modification of the photoelectron (p.e.) final state by scattering from neighboring atoms. For K-edges ($1s$) in single scattering (SS) and harmonic approximations, the absorption coefficient is given by $\mu(E) = \mu_0(E)(1 + \chi(E))$ with μ_0 the embedded atom absorption coefficient and the fine structure χ (EXAFS) given by[22,23]

$$\chi(k) = -\sum_j 3(\hat{\epsilon} \cdot \hat{R}_j)^2 \frac{S_0^2 N_j F_j(\pi, k, R_j)}{kR_j^2} e^{-2k^2\sigma_j^2}$$

$$\times e^{-2R_j/\lambda(k)} \sin(2kR_j + \delta_j(k, R_j)). \quad (1)$$

Here k is the free photoelectron wave number measured relative to the Fermi level, $k = \sqrt{2m(E - E_0)/\hbar^2}$, with E the photon energy and E_0 the absorption threshold for the core electron excitation; $S_0^2 N_j$ is an effective coordination number, which includes changes in the passive electrons' wave functions due to the presence of the core hole; F_j a spherical wave backscattering amplitude; σ_j the root mean squared relative displacement in interatomic distance; λ an effective mean free path, which includes the finite lifetime of the core hole; R_j the interatomic distance; δ_j an overall scattering phase shift; and $\hat{\epsilon}$ the x-rays' polarization vector. The sum is
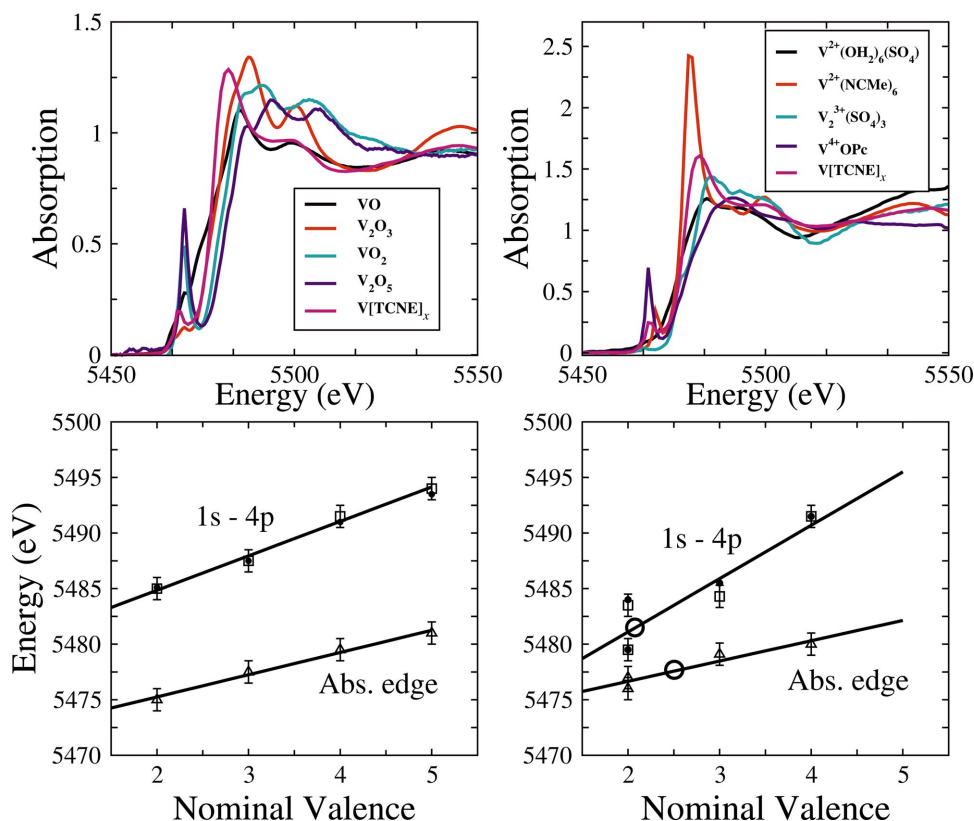
FIG. 2. (Color) Left: V K-edge XANES data on a series of vanadium oxides (top left) and molecular compounds (top right) with known oxidation states of V. The XANES data for $V[TCNE]_x$ are also shown. Energy shifts in absorption edge (maximum derivative) and the $1s \rightarrow 4p$ transition (peak in absorption) are shown for oxides (left bottom) and molecular standards (right bottom). The results for $V[TCNE]_x$ are shown by circles (right bottom).

over all possible single scattering paths. For samples with no preferred orientational ordering, an angular averaging over the relative orientations of the electric field vector of the linearly polarized synchrotron radiation and the bond direction gives $\langle (\hat{\epsilon} \cdot \hat{R}_j)^2 \rangle = 1/3$, and the EXAFS only contains information on the radial part of the partial pair distribution functions. Since the EXAFS is a superposition of oscillatory functions in p.e. momentum space, a Fourier transform (FT) of $\chi(k)$ with respect to $2k$ is related to this pair distribution function about the absorbing atom but "peaks" in this FT appear shifted from the actual interatomic distances due to the k-dependence of the total p.e. phase shift $\delta_j(k)$ in Eq. (1).

The experimental EXAFS, $\chi^{exp}(k)$, is obtained after subtracting the embedded atom absorption background from the measured absorption coefficient[24] and normalizing by the edge step; namely $\chi^{exp}(k) = [\mu(k) - \mu_0(k)]/\Delta\mu_0(0)$. The absorption threshold is selected to be near the midpoint of the edge step. The data were analyzed using the UWXAFS analysis package[25] together with theoretical standards from FEFF6.[26] These standards were generated using a modified version of the structure of vanadyl phthalocyanine (VOPc)[33] which was used to calculate $F_j(k), \delta_j(k), \lambda(k)$. Theoretical standards were also generated using the structure of $[V(NCCH_3)_6]$.[27] Fitting results were independent of the choice of structure used in generating these standards. A theoretical $\chi^{th}(k)$ is constructed whose adjustable structural parameters R_j, N_j, σ^2 are refined against the experimental data

by nonlinear least squares minimization of a reduced χ_ν^2 statistic,[25]

$$\chi_\nu^2 = \frac{N_I}{\nu N} \sum_{i=1}^{N} \left(\frac{|\tilde{\chi}^{th}(R_i) - \tilde{\chi}^{exp}(R_i)|}{\epsilon(R_i)} \right)^2, \quad (2)$$

where the sum is over all pairs of points (real and imaginary parts of the difference are evaluated) in the fitted region of Fourier transformed R-space [$\tilde{\chi}(R)$ is the complex Fourier transform of $\chi(k)$]. Here $N_I = (2\Delta k \Delta r)/\pi + 2$ is the number of independent points in the fitted region,[28] $\nu = N_I - N_P$ the degrees of freedom in the fit, and $\epsilon(R_i)$ the evaluated uncertainty in the numerator's difference of Eq. (2). An overall E_0 shift fitting parameter is used to adjust the $k=0$ reference between experiment and theory. The former is arbitrarily selected to be near the midpoint of the absorption edge.

The EXAFS measurements on $V[TCNE]_x$ were carried out at 10, 120, and 300 K. As discussed later, measurements at several temperatures allow breaking correlations between fitting parameters allowing for a more accurate determination of coordination number. Figure 3 (top) shows the absorption data at the V K-edge of $V[TCNE]_x$ at 10 K. Also shown is the simulated embedded atom absorption, $\mu_0(E)$, which includes frequencies up to 1.0 Å, i.e., below structural frequencies.[24] The derived $\chi(k)$ data, after the removal of μ_0 and normalization by the edge jump, are shown for three independent scans in the bottom panel of Fig. 3. An estimate
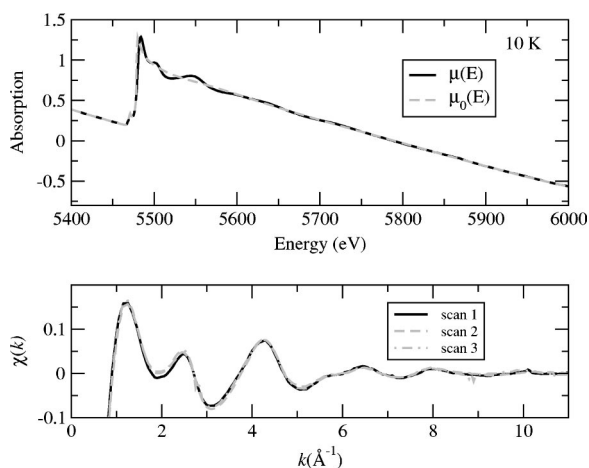
FIG. 3. Top: V K-edge absorption data on V[TCNE]$_x$ at 10 K. The background function $\mu_0(E)$ used to isolate the EXAFS is also shown. Bottom: EXAFS data $\chi(k)$ from three independent scans at 10 K after background removal and normalization.
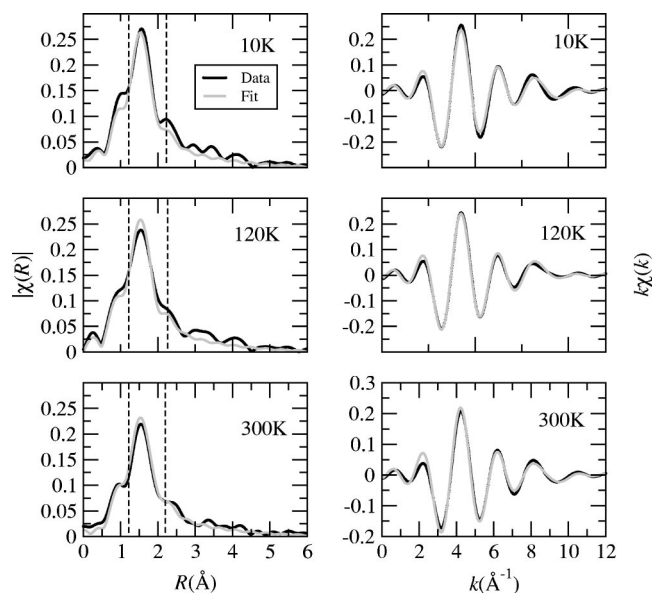

FIG. 4. Amplitude of complex Fourier transform (left) and back Fourier transforms of the fitted region of R-space (right) together with their corresponding fits for data taken at 10, 120, and 300 K. Vertical dashed lines indicate the fitted region, which includes first shell only.

of the noise in the EXAFS data is obtained from the averaged root mean squared variation between these scans, 4.9 $\times 10^{-3}$, which limits the usable k-range from above to ≈ 10 Å^{-1}. Uncertainties in background removal limit the k-range from below to ≈ 2.5 Å^{-1}.

Averaged EXAFS data in a $\Delta k=[2.5-10]$Å^{-1} range was Fourier transformed into real space and fitted in the range $\Delta r=[1.2-2.2]$Å, which includes first shell information only. The total number of independent points in this fitting range is $N_I=6$, while only a total of four fitting parameters are used. Correlations between fitting parameters $E_0, \delta r_j$, which affect the EXAFS phase, and N_j, σ^2, which affect the EXAFS amplitude, were reduced by weighting the EXAFS data by $k^w(w=1,2,3)$ and simultaneously fitting the differently weighted EXAFS, $k^w\chi(k)$, using a single set of structural parameters. This assures that the values obtained for the fitting parameters are physical; i.e., they do not depend on the arbitrary k-weight used in the analysis. While the correlations cannot be removed in the fits, they are affected by weighting since the correlated parameters mentioned above enter the EXAFS equation with different k dependencies. We note that our error analysis includes the effect of correlations between fitting parameters.

First, simultaneous fits of differently weighted EXAFS data were carried out for each temperature independently. Later we fitted the 10, 120, and 300 K data simultaneously by constraining the vibrational disorder σ^2_{vib} in nearest neighbor distance to follow an Einstein model,[29] but allowing for a T-independent offset, σ^2_{off}, to account for static disorder in the interatomic distance, i.e., $\sigma^2=\sigma^2_{\text{vib}}+\sigma^2_{\text{off}}$, or

$$\sigma^2 = \frac{\hbar^2}{2M_r K_B \theta_E}\coth\left(\frac{\theta_E}{2T}\right) + \sigma^2_{\text{off}}, \quad (3)$$

with θ_E the Einstein temperature and M_r the reduced mass of the atoms comprising the bond. The σ^2_{off} term represents T-independent Gaussian disorder not accounted for by the model, such as due to unresolved splitting in the nearest

neighboring distance. The T-dependent constraint for σ^2 further reduces its correlation with N in the fits and diminishes the uncertainties in both fitted parameters.

Figure 4 shows the amplitude of the complex Fourier transforms (left) and the back Fourier transforms to k-space of the first shell region of R-space (right) together with corresponding fits to the data. The passive electron amplitude reduction factor, S_0^2 in Eq. (1), assumed to depend only on the absorbing atom type and not on its environment,[30] was obtained from measurements and fits of a vanadium metal foil to be $S_0^2=0.77(5)$ and set to this value in all other fits. Structural parameters derived from best fits are shown in Table I and partially summarized in Fig. 5. The quality of fit is quantified by the fractional misfit in real space ρ,[31] also included in Table I,

$$\rho = \frac{\sum_{i=1}^N |\tilde{\chi}^{\text{th}}(r_i) - \tilde{\chi}^{\text{exp}}(r_i)|^2}{\sum_{i=1}^N |\tilde{\chi}^{\text{exp}}(r_i)|^2}. \quad (4)$$

TABLE I. Structural parameters for the V-N distance in V[TCNE]$_x$. The number of independent points for all three temperature data sets is $N_I=18$, while a number of $N_P=6$ fitting parameters were used to fit all T-sets. $S_0^2=0.77(5)$ was obtained from fits to a V metal foil; a single energy origin shift parameter was fitted for all temperatures, $E_0=0.5\pm0.5$ eV; the fitted Einstein temperature is $\theta_E=534(54)$ K. The last column shows the misfit fraction ρ defined in the text.

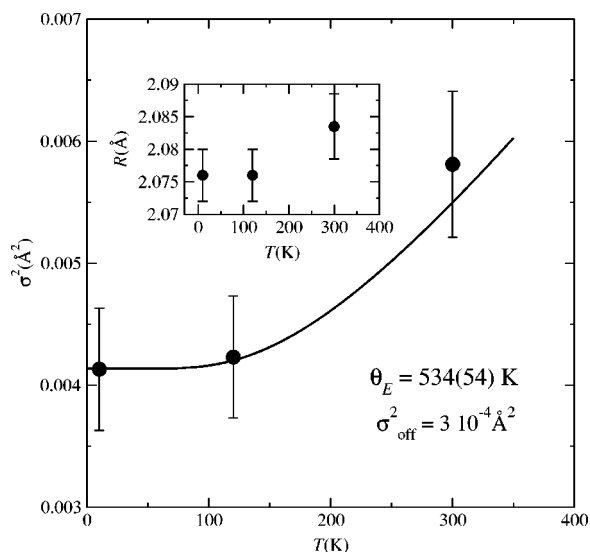| $T(K)$	R(Å)	σ^2(Å^2)	N	ρ
10	2.076(4)	0.0041(5)	6.04±0.25	0.034
120	2.076(4)	0.0042(5)	6.04±0.25	0.025
300	2.084(5)	0.0058(6)	6.04±0.25	0.018

FIG. 5. Temperature dependence of the mean squared disorder in the V-N interatomic distance obtained from the EXAFS fits. Points are from fits to individual data sets; the solid line is from simultaneous fits to all data sets using an Einstein model with static disorder [Eq. (3); the fitted Einstein temperature and static disorder are shown]. The zero-point vibrational component of the Einstein model dominates the disorder, the static disorder σ^2_{off} being about ten times smaller even at the lowest temperature. The inset shows thermal expansion in the V-N distance.

Excellent fits to the data (few % misfit) were obtained for a first coordination shell composed of nitrogen atoms. The fitted V-N distances, disorder, and coordination number as a function of temperature are summarized in Table I. The fitted coordination number, N, is 6.04 ± 0.25. The V-N distance, R, is 2.076(4)Å at 10 K and is 2.084(5)Å at 300 K. This is 0.03 Å shorter than that reported for the model compound $[V(NCCH_3)_6]^{2+},^{32}$ indicating that $V[TCNE]_x$ has more V-N backbonding and a stronger bond than occurs for $[V(NCCH_3)_6]^{2+}$. The temperature-dependent σ^2 corresponds to a characteristic Einstein temperature of $\theta_E=534(54)K$ or an equivalent effective local force constant of $k=87$ N/m.

To further test the accuracy of EXAFS for coordination number determination, we performed measurements and analysis on three reference compounds with known coordination numbers. Data and fits for $(NH_4)_3[VS_4]$, VOPc, and $VCl_3(THF)_3$, with coordination numbers of four, five, and six, respectively, are shown in Fig. 6. In these fits, the known structures of the compounds were used as initial guesses in the refinements.[19,33,34] Small splittings in first-neighbor dis-

TABLE II. Structural parameters for the V-S distance in $(NH_4)_3[VS_4]$. Fitting ranges are $k=[2,12]Å^{-1}$, $R=[1.3,2.2]Å$. The number of total independent points in the three differently weighted data sets is $N_I=20$, while a number of $N_P=4$ fitting parameters were used. $S_0^2=0.77(5)$, obtained from fits to a V metal foil. The mean V-S distance agrees well with $R=2.154(16)Å$ in Ref. 19.

T(K)	R(Å)	σ^2(Å^2)	N	ρ
300	2.142(8)	0.0015(8)	3.93 ± 0.35	0.04

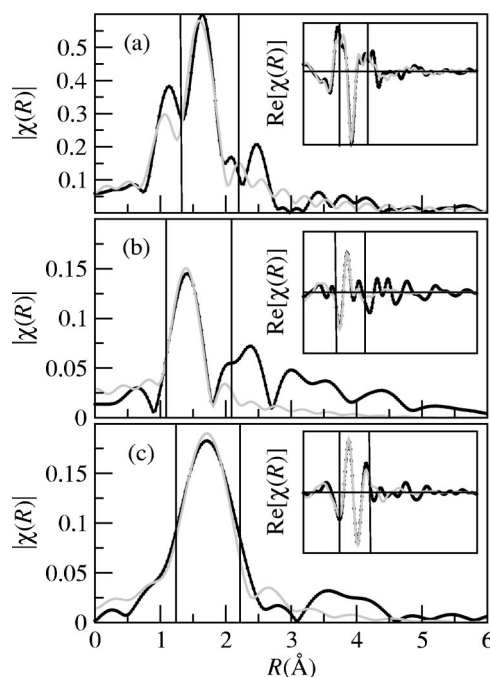

FIG. 6. Amplitude and real part of the complex Fourier transforms of the EXAFS data and fits for (a) $(NH_4)_3[VS_4]$ (b) VOPc, and (c) $VCl_3(THF)_3$. Fitted regions are indicated by vertical lines and include the first shell only. Fitted structural parameters are given in Tables II–IV.

tances beyond the spatial resolution of EXAFS were neglected, and the radial distribution function was represented in those cases by an average interatomic distance, R, and the rms Gaussian disorder σ^2 about that distance. The refined parameters are summarized in Tables II–IV. In all cases the refined coordination numbers and first neighbor distances are in agreement with published values[19,33,34] within error bars.

V. DISCUSSION

Knowledge of the number and type of atoms bound to V is essential in understanding the nature of bonding between V and TCNE. This in turn controls magnetic exchange pathways that result in the remarkably high ordering temperature of this material. A critical parameter regulating magnetic ordering is the sign and magnitude of spin exchange coupling J between V and TCNE spins. While the ordering temperature

TABLE III. Structural parameters for V-O and V-N distances in VOPc. Fitting ranges are $k=[2,10]Å^{-1}$, $R=[1.1,2.1]Å$. The number of independent points in all three differently weighted data sets is $N_I=19$, while a number of $N_P=7$ fitting parameters were used. $S_0^2=0.77(5)$, from fits to a V metal foil. Fit mismatch in real space is $\rho=0.012$. The V-O and V-N mean distances are reported as 1.580(3)Å and 2.026(7)Å, respectively, in Ref. 33.

Bond	R(Å)	σ^2(Å^2)	N
V-O	1.61(2)	0.003(2)	1.10 ± 0.12
V-N	2.01(2)	0.003(2)	4.06 ± 0.43

TABLE IV. Structural parameters for V-O and V-Cl distances in $VCl_3(THF)_3$. Fitting ranges are $k=[3,10]Å^{-1}$, $R=[1.2,2.2]Å$. The number of independent points in all three differently weighted data sets is $N_I=19$, while a number of $N_P=7$ fitting parameters were used. $S_0^2=0.77(5)$, from fits to a V metal foil. The fit mismatch in real space is $\rho=0.005$. The V-O and V-Cl mean distances are reported as 2.08 Å and 2.34 Å, respectively, in Ref. 34.

Bond	R(Å)	σ^2(Å^2)	N
V-O	2.08(1)	0.003(2)	2.8 ± 0.4
V-Cl	2.36(1)	0.003(2)	2.7 ± 0.4

T_c is directly obtained from magnetic measurements, the magnitude of J is obtained from fits to mathematical models (e.g., from mean field theory), all of which require an *a priori* knowledge of the number of nearest neighbor sites.

Careful EXAFS analysis shows that the coordination number of V in $V[TCNE]_x$ is $N=6.04\pm0.25$. This strongly suggests octahedral coordination. The relatively small uncertainty in this number was achieved through simultaneous fits of T-dependent data. We note that the *orientational* arrangement of atoms in the first shell coordination cannot be resolved from these EXAFS measurements since angular information is lost in a powder sample. Nonetheless, a slightly distorted octahedral geometry is consistent with the XANES results and is by far the most common geometry for coordination of six, especially for V in the 2+ valence state.

The valence state of V was found from XANES measurements to be in the vicinity of 2+. The interpolation scheme based on molecular standards with known valence states yields a valence of 2.25 ± 0.25. This result is in good agreement with surface sensitive x-ray photoelectron spectroscopy (XPS),[3] which finds a predominant 2+ state. A minority 5+ oxidation component, which increases upon air exposure, was attributed in the XPS work to V_2O_5 surface contamination. Since the XANES measurements are bulk measurements (surface insensitive), they provide independent confirmation of the XPS results of a predominant 2+ oxidation state.

An intrinsic difficulty of x-ray absorption techniques is the presence of a core hole in the excited final state. Although very short lived ($\approx 1fs$), the electrostatic potential introduced with the core hole causes a redistribution of electronic charge density, the details of which strongly depend on the ability of valence electrons to effectively screen this potential. In other words, the renormalization of energy levels introduced by the core-hole potential depends on the ionicity (covalency) of the chemical bond in which the absorbing atom takes part. Hence, standards used in empirical methods for chemical valence determination based on interpolation schemes should involve compounds with similar chemical bonding.

We demonstrated in Sec. III that the use of inappropriate standards, such as highly ionic vanadium oxides, leads to inconsistent results for the valence state of V in $V[TCNE]_x$. While the use of molecular standards yielded a good degree of self consistency in valence determination based on chemical shifts of different absorption features, the accuracy is not
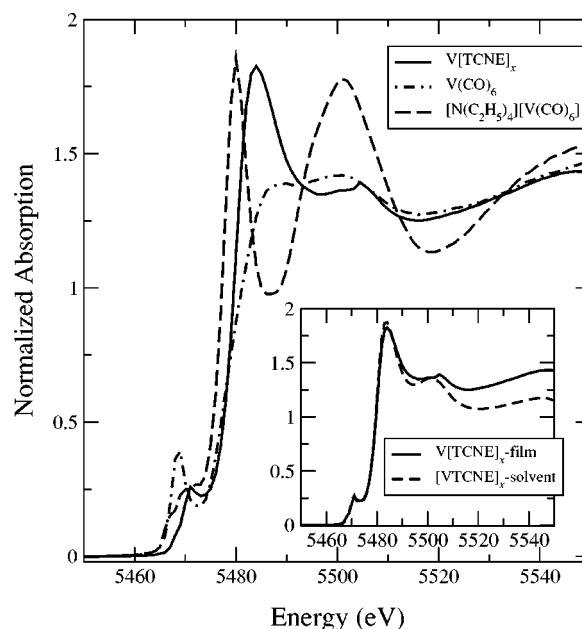

FIG. 7. XANES spectra for $V[TCNE]_x$ (solvent-free) together with those for $V(CO)_6$ and $[N(C_2H_5)_4][V(CO)_6]$. The inset shows XANES spectra for $V[TCNE]_x$ grown by chemical vapor deposition (solvent free) and in a CH_2Cl_2 solution.

better than a quarter of a valence electron. We believe most of the uncertainty comes from the different electronegativities of coordinating atom types in the known standards introducing variations in the extent of screening of the core-hole potential in the excited state. For example, the different position of the $1s \rightarrow 4p$ feature for $[V^{II}(NCCH_3)_6][B(C_6H_5)_4]_2$ and $V^{II}(OH_2)_6(SO_4)$ standards is probably due to the different coordinating atom types (six N and six O, respectively). Although we cannot rule out a mixed valence state for V based on the uncertainty quoted above, the lack of significant static disorder in V-N distances, together with the lack of significant broadening in the leading absorption edge, support a single valence state for V. A mixed valence state is expected to result in dissimilar local structures and an associated increase in the spread of V-N distances.

The clear presence of a pre-edge feature in the XANES spectrum of $V[TCNE]_x$, albeit small, indicates the breaking of inversion symmetry at the V -site. Figure 7 compares the XANES data for $V[TCNE]_x$, $V(CO)_6$, and $[N(C_2H_5)_4] \times [V(CO)_6]$. The structure of $V(CO)_6$ is very close to a regular octahedron, although there is a marginally significant tetragonal Jahn-Teller distortion leading to 1.993(2)Å V-C axial distances and 2.005(2) Å V-C equatorial distances.[21] This small splitting of about ±0.006 Å about an average distance of 1.999 Å breaks the V -site inversion symmetry and gives rise to the observed pre-edge feature. Although the structure of $[N(C_2H_5)_4][V(CO)_6]$ has not been reported, similar deviations from octahedral symmetry are expected in this compound based on the reported structures of $V^{II}[CN-t-C_4H_9]_6[V^{-I}(CO)_6]_2(V^{II}-C=2.10$ Å, $V^{-I}-C=1.92$ Å),[35] and $[N(PPh_3)_2][V(CO)_6](V^{-I}-C=1.93$ Å).[36] Since the size of the pre-edge feature is directly related to the deviation from regular octahedral geometry we conclude,

based on Fig. 7, that the size of the distortions away from O_h symmetry in V[TCNE]$_x$ are comparable to those in V(CO)$_6$, assuming all V sites are equivalent. An alternative explanation for the origin of the pre-edge feature involves the coexistence of inequivalent vanadium environments, e.g., those with O_h symmetry and those in defected structures. Since the XANES data is a weighted average over all local environments, we cannot rule out a small fraction of defected V sites giving rise to the observed pre-edge peak despite a majority of V sites exhibiting O_h symmetry. Since at present we lack models for these hypothetical defected sites we cannot estimate their fraction, which should result in average coordination numbers, distances, and disorder consistent with those derived from the EXAFS analysis. Finally, we note that zero-point and thermal atomic motion can contribute to the pre-edge peak intensity. Since the time scale of lattice dynamics ($\approx 10^{-13}$ s) is longer than the core-hole lifetime ($\approx 10^{-15}$ s) during which the structure is probed, instantaneous breaking of centrosymmetry by thermal and zero-point motion can result in a small pre-edge peak, as observed in centrosymmetric EuTiO$_3$.[37] However, the sizable pre-edge peak of V[TCNE]$_x$ cannot be explained by thermal disorder alone and requires one of the mechanisms discussed above.

We note that EXAFS analysis cannot resolve the presence of small splittings in the radial distribution function due to its limited spatial resolution. The smallest splitting in interatomic distance that can be resolved (distinguished as two separate distances) is given by $\delta r \approx \pi/2k_{max}$, where k_{max} is the maximum photoelectron (p.e.) wave number in the data. In other words, a difference in p.e. phase shift of $\approx \pi$ is needed (the p.e. travels twice the interatomic distance between the absorber and the scatterer before recombining with its outgoing part at the absorber). Since $k_{max} = 10$ Å, the spatial resolution of 0.16 Å is much more coarse than the estimated splitting. This is not to be confused with the much more accurate determination of *average* interatomic distances by EXAFS, of about 0.005 Å.

Unresolved differences in V-N distances would manifest in broadening of the radial distribution derived from EXAFS. Our model allows for such intrinsic Gaussian broadening in the form of a σ_{off}^2, which fits to 3×10^{-4} Å^2 (Fig. 5). This gives an upper limit for unresolved splittings in V-N distances of 0.017 Å, well within the estimates based on the size of the XANES pre-edge feature. A comparison of XANES data for solvent-free, CVD-grown V[TCNE]$_x$ and that prepared via the reaction of V[TCNE]$_x$ and V(CO)$_6$ in CH$_2$Cl$_2$ is shown in the inset of Fig. 7. The nearly identical pre-edge features in both V[TCNE]$_x$ samples is consistent with CH$_2$Cl$_2$ not binding to V. The EXAFS measurements on the solvent-containing sample confirm this idea as the EXAFS data are consistent with a first neighboring environment to V composed of 6 nitrogens at 2.11(2)Å, i.e., nearly the same local structure as the solvent free sample. Since both compounds have the same magnetic ordering temperatures, it is reasonable to assume that the nature of the nearest neighboring environment plays a crucial role in determining the magnetic ordering temperature.

The high degree of local order in the coordination environment of V ions is evidenced in the sharpness of the radial distribution function of V-N distances. The rms variation in this distance is 0.076 Å compared to 0.039 Å for V-S distances in strongly covalent (NH$_4$)$_3$[VS$_4$] and about 0.054 Å for V-O, V-N, and V-Cl distances in VOPc and VCl$_3$(THF)$_3$ (Tables II–IV). This small disorder is indicative of strong binding betwen V and TCNE. The V-N bond is characterized by an effective local force constant of $k = 87$ N/m $= 5.5$ eV/Å^2. This is only a factor of two weaker than the effective force constants for V-O and V-N in strongly covalent VOPc(~ 160 N/m) and a factor of three stronger than the effective spring constant for Cu-Cu neighbors in Cu metal.[38]

The small disorder in V-N distances is likely to be important in determining the high magnetic ordering temperature of V[TCNE]$_x$ since the magnetic ordering temperature scales with the strength of exchange coupling between spins. In a simple picture of structurally disordered magnetic materials, $T_c \sim \int r^2 g(r) J(r) dr$, where $r^2 g(r)$ is the radial distribution function. A narrow radial distribution function, like the one obtained for V-N distances with negligible static disorder, is an important element in promoting high T_c. In addition, the strong V-N bonding and a 3-D network structure are responsible for the insolubility of the V[TCNE]$_x$ in organic solvents.

VI. SUMMARY AND CONCLUSIONS

X-ray absorption spectroscopy was used to determine the chemical oxidation state and local coordination environment of V in the V[TCNE]$_x$($x \approx 2$) molecule-based magnet. The oxidation state of about 2+ obtained by this bulk-sensitive technique is consistent with previous surface sensitive measurements using x-ray photoelectron spectroscopy. Although a mixed valence state for vanadium cannot be ruled out, a lack of intrinsic broadening in the leading absorption edge and radial distribution function of V-N distances suggest a single V oxidation state. The V ions are coordinated by six N ions, most likely in a slightly distorted octahedral environment. The strong binding between V and TCNE and a 3-D network structure are responsible for the insolubility of this magnet in organic solvents. Solvent-containing (CH$_2$Cl$_2$) and solvent-free V[TCNE]$_x$ magnets, which have similar magnetic ordering temperatures above room temperature, exhibit the same local coordination by six nitrogens. This local coordination seems to facilitate the remarkably strong magnetic interactions present in this family of molecule-based magnets.

*Email address: haskel@aps.anl.gov

[1] J. M. Manriquez, G. T. Yee, R. S. McLean, A. J. Epstein, J. S. Miller, Science **252**, 1415 (1991).

[2] J. Zhang, C. Vazquez, P. Zhou, W. B. Brinckerhoff, R. S. McLean, J. S. Miller, and A. J. Epstein, Am. Chem. Soc. Sym. Series **644**, 311 (1996).

[3] K. I. Pokhodnya, A. J. Epstein, and J. S. Miller, Adv. Mater. (Weinheim, Ger.) **12**, 410 (2000). $V(CO)_6$ was prepared prior to use from $[N(C_2H_5)_4][V(CO)_6]$ (see Ref. 14), which was obtained from Strem Chemicals.

[4] P. Zhou, S. M. Long, J. S. Miller, and A. J. Epstein, Phys. Lett. A **181**, 71 (1993).

[5] P. Zhou, B. G. Morin, J. S. Miller, A. J. Epstein, Phys. Rev. B **48**, R1325 (1993).

[6] K. I. Pokhodnya, D. A. Pejakovic, A. J. Epstein, and J. S. Miller, Phys. Rev. B **63**, 174408 (2001).

[7] J. Zhang, J. Ensling, V. Ksenofontov, P. Gutlich, A. J. Epstein, J. S. Miller, Angew. Chem., Int. Ed. **37**, 657 (1998).

[8] M. A. Girtu, C. M. Wynn, J. Zhang, J. S. Miller, and A. J. Epstein, Phys. Rev. B **61**, 492 (2000); K. I. Pokhodnya, N. Petersen, and J. S. Miller, Inorg. Chem. **41**, 1996 (2002).

[9] V. N. Prigodin, N. P. Raju, K. I. Pokhodnya, J. S. Miller, and A. J. Epstein, Adv. Mater. (Weinheim, Ger.) **14**, 1230 (2002).

[10] K. I. Pokhodnya, V. Burtman, A. J. Epstein, J. W. Raebiger, and J. S. Miller, Adv. Mater. (Weinheim, Ger.) **14**, 1211 (2003).

[11] D. A. Pejakovic, C. Kitamura, J. S. Miller, and A. J. Epstein, Phys. Rev. Lett. **88**, 057202 (2002).

[12] A. L. Tchougreeff and R. Hoffmann, J. Phys. Chem. **97**, 350 (1993).

[13] A. L. Ankudinov, B. Ravel, J. J. Rehr, and S. D. Conradson, Phys. Rev. B **58**, 7565 (1998); E. A. Stern, *ibid.* **10**, 3027 (1974); R. Garde, F. Villain, and M. Verdaguer, J. Am. Chem. Soc. **124**, 10531 (2002).

[14] J. E. Ellis, R. A. Faltynek, G. L. Rochfort, R. E. Stevens, and G. A. Zank, Inorg. Chem. **19**, 1082 (1980).

[15] S. J. Anderson, F. Wells, G. Wilkinson, Polyhedron **7**, 2615 (1988).

[16] M. Kranz, D. E. Goldberg, A. Ribner, Inorg. Synth. **7**, 94 (1963).

[17] R. T. Claunch, M. M. Jones, and W. C. Wolsey, Inorg. Synth. **7**, 138 (1963).

[18] L. E. Manzer, J. Deaton, P. Sharp, and R. R. Schrock, Inorg. Synth. **21**, 92 (1982).

[19] Y. Do, E. D. Simhom, and R. H. Holm, Inorg. Chem. **24**, 4635 (1985).

[20] J. Wong, F. W. Lytle, R. P. Messmer, and H. H. Maylotte, Phys. Rev. B **30**, 5596 (1984).

[21] S. Bellard, K. Rubinson, and G. Sheldrick, Acta Crystallogr., Sect. B: Struct. Crystallogr. Cryst. Chem. **35**, 271 (1979).

[22] E. A. Stern, Phys. Rev. B **10**, 3027 (1974).

[23] P. A. Lee and J. B. Pendry, Phys. Rev. B **11**, 2795 (1975).

[24] M. Newville P. Livins, Y. Yacoby, J. J. Rehr, and E. A. Stern, Phys. Rev. B **47**, 14126 (1993).

[25] E. A. Stern, M. Newville, B. Ravel, Y. Yacoby, and D. Haskel, Physica B **208–209**, 117 (1995).

[26] S. Zabinsky, J. J. Rehr, A. Ankudinov, R. C. Albers, and M. J. Eller, Phys. Rev. B **52**, 2995 (1995).

[27] P. Chandrasekhar and P. H. Bird, Inorg. Chim. Acta **97**, L31 (1985).

[28] E. A. Stern, Phys. Rev. B **48**, 9825 (1993).

[29] E. Sevillano, H. Meuth and J. J. Rehr, Phys. Rev. B **20**, 4908 (1979).

[30] J. J. Rehr, E. A. Stern, R. L. Martin, and E. R. Davidson, Phys. Rev. B **17**, 560 (1978); E. A. Stern, B. A. Bunker and S. M. Heald, *ibid.* **21**, 5521 (1980).

[31] M. Newville, B. Ravel, D. Haskel, J. J. Rehr, E. A. Stern, and Y. Yacoby, Physica B **208–209**, 154 (1995).

[32] P. B. Hitchcok *et al.*, J. Chem. Soc. Dalton Trans. **1994**(24), 3683 (1994); P. Chandrasejhar and P. H. Bird, Inorg. Chim. Acta **97**, L31 (1985); Z. Janas *et al.*, Organometallics **19**, 4252 (2000).

[33] R. F. Ziolo, C. H. Griffiths, and J. M. Troup, J. Chem. Soc. Dalton Trans. **7**, 2300 (1980).

[34] U. Englert, F. Calderazzo, and G. Pampaloni, **8**, 237 (1997); F. A. Cotton, S. A. Duraj, M. W. Extine, G. E. Lewis, W. J. Roth, C. D. Schmulbach, and W. Schwotzer, J. Chem. Soc., Chem. Commun. **23**, 1377 (1983).

[35] L. D. Silverman, P. W. R. Corfield, and S. J. Lippard, Inorg. Chem. **20**, 3106 (1981).

[36] R. D. Wilson and R. Bau, J. Am. Chem. Soc. **96**, 760 (1974).

[37] B. Ravel and E. A. Stern, Physica B **209**, 316 (1995).

[38] A. V. Poiarkova and J. J. Rehr, J. Synchrotron Radiat. **6**, 313 (1999).